

# Model of a Filament Assisted CVD reactor

Jozef Brcka\*

TEL US Holdings, Inc., Technology Development Center

\*Corresponding author: 255 Fuller Rd., Albany, NY 12203, jozef.brcka@us.tel.com

**Abstract:** In this presentation we are dealing with the computational fluid model of a Filament Assisted Chemical Vapor Deposition (FACVD) reactor. Proposed strategy in this study involved several steps: (a) development a computational model for FACVD process capable to describe and obtain with reasonable accuracy all relevant phenomena occurring in the reaction chamber; (b) validation the computational model predictions with experimental data; and (c) analyzing and testing the effects of process conditions, boundary conditions on deposition performance by model on overall performance of the FACVD reactor. Here, we were dealing mostly with the first step, only partially touching the next two.

Presented model was built under COMSOL Multiphysics environment (v.3.5) in 2D Cartesian coordinate system. Model is utilizing following modules: Incompressible Navier-Stokes Module, General Heat Transfer Module, and Convection and Diffusion Modules for individual species. Bulk chemistry is relatively simple considering surface mechanism as dominant in film growth description. At this moment a limited surface model is incorporated into boundary conditions due to its complexity and non-linearity. The results and assumptions considered in heat transfer model (radiation from multi-line heating source) and diffusion model are discussed, the reactor flow field, distribution of the products concentration and their influence on reactor performance are analyzed. Model serves as a pivotal case for building up more complex chemistry and physics into a virtual reactor and provide predictive thesis to be validated by experiment.

**Keywords:** FACVD, polymer films, air gap technology, modeling, low-k interconnect.

## 1. Introduction

Recently, an advanced concept on deposition of a decomposable polymer and a porous low-k organosilicate cap by Filament-Assisted Chemical Vapor Deposition (FACVD) was demonstrated for back-end-of-line (BEOL)

applications in ICs manufacturing.<sup>1</sup> This approach allows to build air gap (AG) structures to reduce the effective dielectric constant in Cu/low-k interconnects. Main feature of this technology includes the fact of low-temperature plasma-free film deposition which offers great advantage against conventional plasma-enhanced CVD (PECVD).<sup>2,3</sup> Last one can produce a degradation in film properties (dangling bonds presence, trapping free radicals, etc.) due to the energetic ion bombardment and VUV radiation.<sup>4</sup> The other applications of a FACVD are expanding from interconnect processing<sup>5</sup> towards a novel areas including novel organic devices, bio-passivation applications, 3D interconnect structures, and energy. For example, stacked films of silicon nitride ( $\text{SiN}_x$ ) and silicon oxynitride ( $\text{SiO}_x\text{N}_y$ ) films deposited at 80°C or less have demonstrated low water vapor transmission rates as well as high transparency and low stress<sup>5</sup> and thus are applicable in gas barriers on polymeric materials. Or deposited by this method the antimicrobial polymer coatings exhibited 99.9999% effectiveness against *E. coli* and *B. subtilis* bacteria.<sup>6</sup>

In the FACVD process regime, filament temperature and choice of process pressure strongly influence the degree of a precursor fragmentation (radical formation), gas phase nucleation, and deposited film morphology. Typically, the precursor(s) is entering reactor in pre-mixed composition and transported by carrier gas. The actual decomposition of reactant occurs within "hot zone" (HZ) from where the products are transported towards the surface. Surface processes and reactions will determine the resulting film properties and deposition performance. Generic process flow that illustrates precursor decomposition is shown in Fig. 1. In dependence on the precursor properties, temperature and pressure, the complex interaction between fluid dynamics and fast chemical reactions can significantly impact the reactor performance on large size silicon wafers.

Substrate temperature governs surface adsorption/desorption and cross-linking of the adsorbed radicals. In specific cases, additional

component (initiator, porogen, etc.) is added into a mixture to initiate and sustain surface processes under required conditions – it is so called initiated CVD (iCVD) deposition regime.<sup>7-10</sup> Both in FACVD and iCVD the deposition of the polymerized film occurs at low wafer temperature, typically much below 100 °C.

Parameters like an average length of polymer chains, the molecular weight distribution, cross-linking, and chain-branching will depend on process parameters, thus affecting the uniformity, yield, and throughput for specific application. The complexity of the processes involved in a FACVD reactor is relatively high, thus computational reactive fluid dynamics (CFD) models are very useful tools in the analysis of such systems. Whereas many studies have focused on a development of the comprehensive or diverse chemistry<sup>11</sup> and mathematical formulation of the problem, to the author's knowledge no work has been published on the use of the formulation the method for

engineering analysis of low-temperature FACVD or iCVD processes, except the most recent ones, for example, the work on the power consumption analysis for an iCVD reactor.<sup>12</sup> Modeling and computational results of FACVD reactive environment, thermal and fluid flow analysis are important means for better understanding the phenomena in industrial level 300 mm FACVD/iCVD reactor.

Proposed strategy in this study involved several steps: (1) Development a computational model for FACVD process capable to describe and obtain with reasonable accuracy all relevant phenomena occurring in the reaction chamber. (2) Validation the computational model predictions with experimental data for gas temperature, and gas-phase concentrations, gas velocity and growth rate inside the reaction chamber. (3) Analyzing and testing the effects of the process conditions, boundary conditions on deposition performance, utilization the model in overall performance of the FACVD reactor.

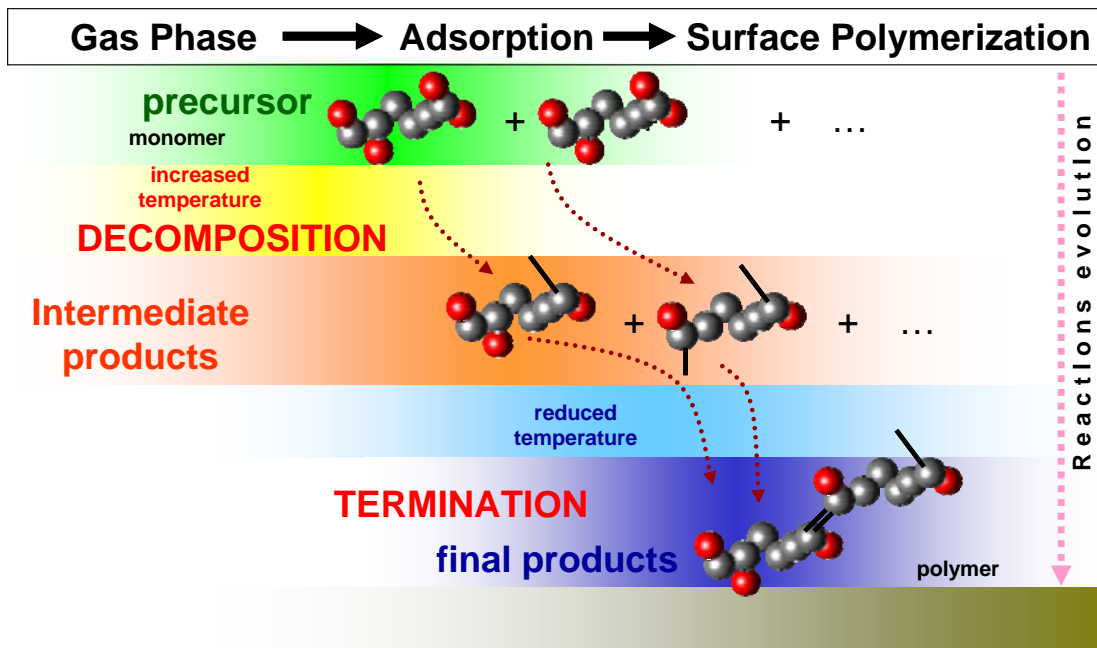


**Figure 1.** Generic mechanism for Filament Assisted Chemical Vapor Deposition (FACVD).

## 2. Use of COMSOL Multiphysics

Presented model was built under COMSOL Multiphysics environment (v.3.5) in 2D Cartesian coordinate system. Choice of the model geometry was based on several

assumptions that are discussed in more details below (Sect. 3.2). Independently, the 2D axial symmetry and 3D case were investigated. However, the results of such study are not included in this work. Model is utilizing following modules: Incompressible Navier-

Stokes Module, General Heat Transfer Module, and Convection and Diffusion Modules for individual species. Computational and coupling structure is illustrated in Fig. 2-a. Variables in a gas flow module are coupled to the temperature computed in heat transfer module. The bulk chemistry is formulated in very simple scheme – only 3 components are considered in carrier gas.

Individual convection and diffusion modules are implemented for monomer, initiator and products of their decomposition. This approach was chosen to switch easily between various process conditions – emulating by model a virtual single chamber processing tool - and used formalism from Fig. 2-b.

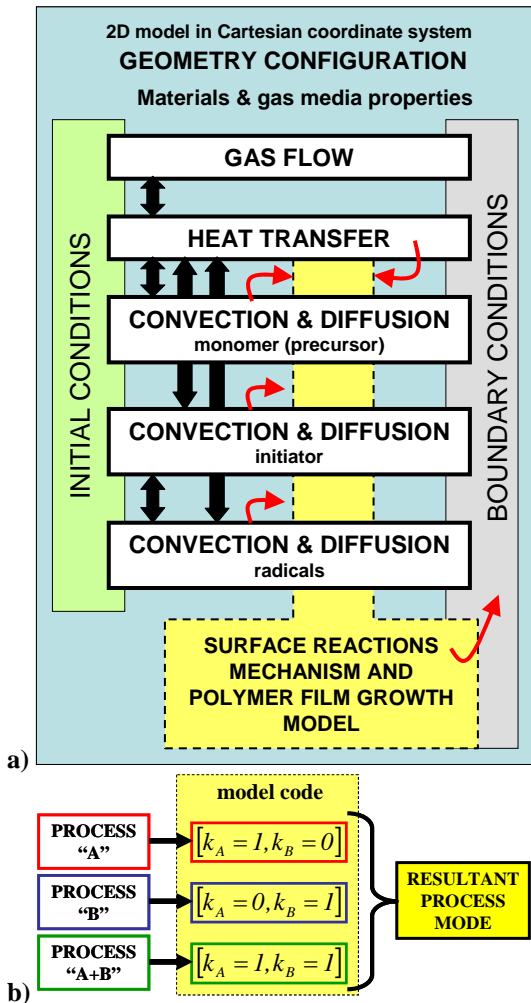


**Figure 2.** FACVD model structure: (a) Computational and coupling scheme of the FACVD model; (b) Simplified logic switch scheme to run diverse chemistry DOE.

Surface model is incorporated into boundary conditions. More complex surface coverage fraction model will be discussed briefly in presentation. The results and assumptions considered into heat transfer (radiation from multi-line heating source) and diffusion model are discussed in Sect. 3.3, the reactor flow field, distribution of the products concentration and their influence on reactor performance are analyzed in subsequent sections. Model serves as a pilot case for building up more complex chemistry and physics into virtual reactor and provide predictive thesis to be validated by experiment.

### 3. Model Description

#### 3.1 Chemistry

Deposition of a decomposable polymer (DP) with desired properties for air gap integration is operating in the iCVD process regime. In this study, we considered a gas mixture consisting of a monomer and initiator in carrier gas which is assisting the precursors to enter and get transported through a reactor. Ethylene glycol diacrylate (EGDA),  $C_8H_{10}O_4$ , was chosen as the monomer precursor, and tert-butyl peroxide (TBPO),  $C_8H_{18}O_2$ , was used as the radical initiator. Selected physical properties of EGDA and TBPO are briefly listed below.<sup>13-15</sup>

The EGDA molecular weight is 170.1626 g/mole, the boiling point 503 K, the gas specific density 5.87488, the liquid molar volume at 298 K is 0.15614  $m^3/kmol$ , and refractive index about 1.4529-1.461.

The TBPO molecular weight is 146.23 g/mole, the gas specific density 5.0486, refractive index about 1.389, and decomposition temperature 190 °C. Heat capacity is in range from 158 to 493  $J.mol^{-1}K^{-1}$  within 200 K to 1000 K interval; the thermal conductivity from 0.0886 to 0.0086  $W.m^{-1}K^{-1}$  within 250 K to 1000 K; viscosity 211 to 54  $\mu P$  within same temperature range.

Temperature dependent parameters are described in next section. We continue collect the available data on physical properties of the complex precursors, which may be potential candidates for diverse film preparation.

Initiating radicals are produced by decomposition of the TBPO within the "hot zone" (< 300 °C) and then transported together with the EGDA monomer in carrier gas (Ar) to

the wafer surface by convective flow and diffusion. At the wafer surface the initiator is activating efficient polymerization of a monomer until the film growth is not terminated. Thus, the generation and distribution of the initiator radicals are crucial in polymerized film formation. As it is typical for iCVD process, the initiator utilization is quite high (80-90%). Active control of substrate temperature modulates the adsorption/desorption rate and the subsequent polymerization reaction. Under specific conditions of the EGDA and TBPO mass flows, the typical deposition rates may exceed over 1  $\mu\text{m}/\text{minute}$ .

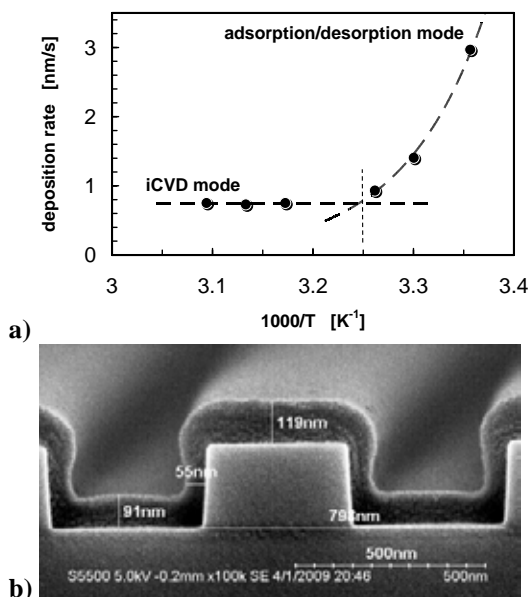


**Figure 3.** Deposition rate of the EGDA monomer in the presence of the TBPO initiator (total pressure was 2 Torr): (a) deposition rate vs. inverse temperature of the substrate; (b) conformal step coverage of the trench feature (substrate temperature was 40 °C).

Dependence of the deposition rate on the substrate temperature under specific conditions is shown in Fig. 3-a. At fixed mass flow rate of the initiator and a low substrate temperature the adsorption/desorption mode is dominant. It is believed, a mono- or multilayer adsorption is occurring at the substrate surface and due to a low desorption rate the propagation phase of the film growth is not running efficiently. Increased substrate temperature provides conditions when TBPO is initiating adsorbed monomer film more efficiently – and the growth occurs through propagation mechanism – the iCVD mode.

Resultant film and coverage of the steps on the substrate are shown in Fig. 3-b.

### 3.2 Reactor Geometry

Actual reactor has a cylindrical shape and it contains a substrate holder with wafer, a heater assembly, a flow plate (showerhead) and flow restriction shield. Gas inlets are situated on the top end of the reactor, and bottom end is in part represented by the wafer, which is evoking immediately a suggested model concept that should consist of a 2D axial symmetry.

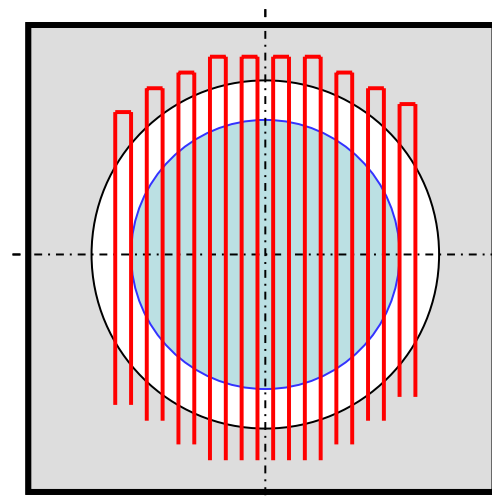


**Figure 4.** Top view of a heater configuration.

On the other hand, the reactor has an intrinsic asymmetry in terms of a multi-line planar heater structure (Fig. 4), which would indicate the utilization of the 3D model for thermal simulation. Heater assembly consists of multiple ribbon pairs (made of NiCr with ribbon size 5 x 0.13 mm) that extend over the 300 mm wafer size.

As we found out from independent 3D thermal simulations,<sup>16</sup> the utilization of 2D axial symmetry was good enough representation of the reactor zone with multi-line heater assembly and is applicable for process evaluation. From engineering viewpoint, the most accurate modeling assessment of a particular heater could be gained by 3D model, however, we know that in combination with the gas flow and the chemistry computation it will increase substantially the requirements on computational resources.

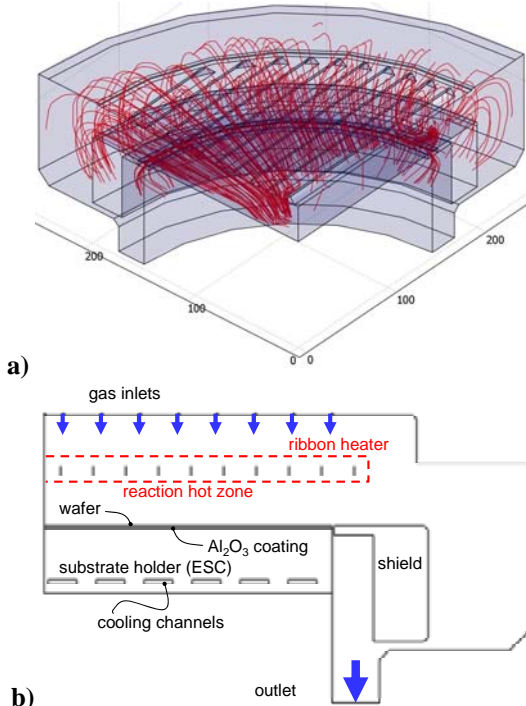


**Figure 5.** Reactor geometry: (a) Cut-off portion of the FACVD reactor in 3D with computed velocity field streamlines; (b) the 2D cross section of the proposed FACVD reactor used in a computational model.

In respect to flow simulation, when we tested a specific inlet flow plate - it contains parallel channels for gas introduction - it was shown that 3D model (or at least 2D in Cartesian coordinate system) would be definitively more accurate for gas flow simulation. Though 3D flow cases were computable (example is shown in Fig. 5-a), in this study the memory limitation and computational time restrictions were major reasons to simplify geometry into 2D Cartesian coordinate system (Fig. 5-b). We are aware, that approximation by 2D model in Cartesian coordinate may require additional post-processing of the results that are dependent on the radial position.

### 3.3 Computational model and parameters

#### Heat Transfer Model

Mathematical model for a heat transfer is using a steady-state heat equation (General Heat Transfer Module)

$$\vec{\nabla} \cdot (-k_d \vec{\nabla} T + \rho_d C_d T \vec{u}) = Q_d \quad (1)$$

where  $T$  is the temperature, and local parameters  $k_d$ ,  $\rho_d$ ,  $C_d$  and  $Q_d$  are thermal conductivity, density, specific heat capacity, and a heat source/sink in each specific domain " $d$ " according definitions in Fig. 5-b. Walls and showerhead temperature were sustained at moderately higher temperature ( $\sim 80$  °C) than substrate ( $\sim$  room temperature). Heating power delivered into NiCr ribbons was up to  $100 \text{ W/cm}^3$ . It is important to mention that normal spectral emissivity of pure NiCr 80 with the presence of slight oxide is from 0.35 to 0.4, while the emissivity of heavily oxidized NiCr 80 is in the range of 0.85 to 0.9, see Ref.<sup>17</sup>, and it may depend on the temperature.<sup>18</sup> This behavior will have impact on the ribbon's temperature under given conditions.

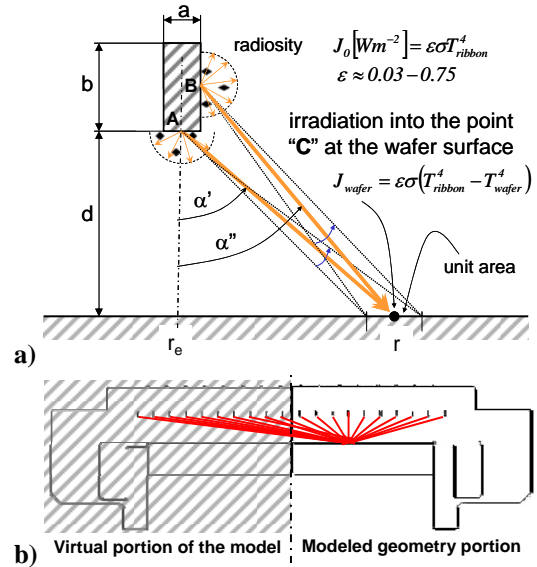


**Figure 6.** Radiation model: (a) Radiosity considered in model; (b) Configuration of radiation sources to account for complete irradiation effect.

The irradiation of the wafer surface in point "C" from an individual heating element is illustrated in Fig. 6-a. The radiant losses were assumed at the ribbon surface and accounted as a heat source due to irradiation of the wafer. Radiosity from a single ribbon was estimated by relation

$$G_C^e \approx G_{AC}^e + G_{BC}^e \quad (2)$$

where

$$G_{AC}^e = \frac{adJ_0\Delta\omega_{u.a.}}{2\pi[d^2 + (r - r_e)^2]^{3/2}} \quad (3)$$

$$G_{BC}^e = \frac{adJ_0\Delta\omega_{u.a.}}{2\pi[d^2 + (r - r_e)^2]^{3/2}} \times \frac{b(d + b/2)}{ad \left[ \frac{(d + b/2)^2 + (r - r_e)^2}{d^2 + (r - r_e)^2} \right]^{3/2}} \quad (4)$$

and

$$\Delta\omega_{u.a.} \sim \left[ 1 + (r - r_e)^2 / d^2 \right]^{-1/2} \quad (5)$$

Meanings of the other symbols is obvious from Fig. 6-a. The expressions (2) to (5) can be simplified substantially in design where dimensions comply with relation  $d \gg b \gg a$ .

To estimate the radiosity, an instant temperature of the ribbons was assessed by readings given in Point Integration Variables command applied on ribbon domains. Nevertheless, the computing is accomplished only at one half of the reactor, we have assumed involvement of both symmetric components in the reactor geometry, that is both “modeled” and “virtual” portion of the model (see Fig. 6-b). We believe, this is an important factor for correct temperature assessment on the wafer. Also this feature allowed us to investigate the impact of the positioning the ribbon, their deviation from correct position due to their prolongation, thermal expansion or twisting.

Integral irradiation power,

$$G_C = \sum_e G_C^e \quad (6)$$

at wafer surface is shown in Fig. 7-a. The illustration of impact on the irradiation due to ~10 % variation of the temperature at a single ribbon is shown in Fig. 7-b. One more step in model improvement in terms of the irradiation will include an integration along the heating lines. This approach will eliminate need for full 3D thermal model we discussed earlier.

Silicon wafer was placed on a substrate holder made of aluminum with water cooling channels and coated by alumina on the top. Due to high-flow rate of cooling water, the channels can be set inactive in model and constant temperature is assigned to their boundaries. Formally, we used ceramic coating with thickness 1 mm. Thermal properties that would reflect actual thickness (up to several microns) are adjusted by alumina thermal properties. Reason to include full

domain for substrate holder in the bottom of the assembly was to account better for wafer heating due to the irradiation from heater assembly, thus to interpret temperature and its impact on surface reactions at the wafer in more realistic way.

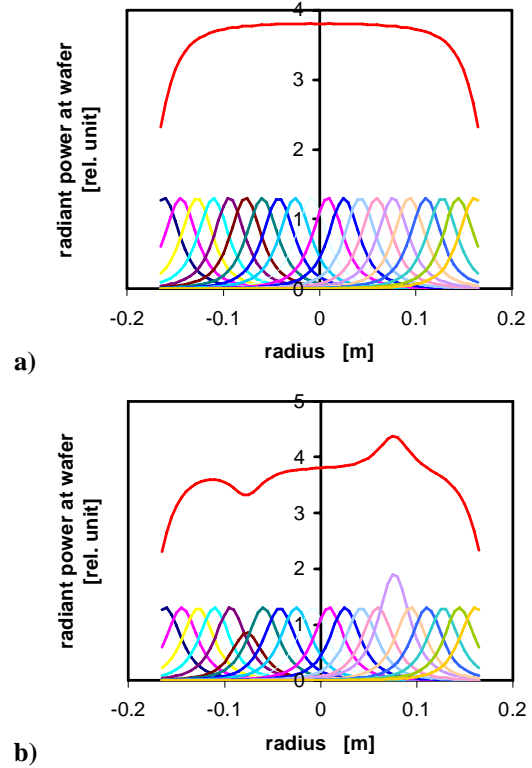


**Figure 7.** Profile of the irradiation power at wafer surface from (a) ideal and uniform heater assembly, and (b) temperature is off-set at individual heater lines to  $\pm 10\%$ .

### Precursor Transport Model

Gaseous media flow is described by steady-state incompressible Navier-Stokes equation. Velocity of the entering gas mixture was estimated based on a consumption of the mixture components and a geometry of the flow plate. Typically, the EGDA consumption was about several g/hour in 100 sccm carrier gas (Ar) and TBPO up to 100 sccm in 50-200 sccm carrier gas flow (Ar). Top plate with uniform distribution of over 200 holes ( $\varnothing 1$  mm) provided gas velocity at the inlet in range from 0.3 to 0.5 m/s. The purpose of an annular shield was to restrict the gas flow directly to the

pumping outlet and provide better control over the process parameters.

Viscosity of the precursors was estimated by relations<sup>19</sup>

$$\eta_{EGDA} \approx 5.7 \times 10^{-13} T^2 + 1.985 \times 10^{-8} T + 5.657 \times 10^{-7} \quad (7)$$

$$\eta_{TBPO} \approx -3.729 \times 10^{-12} T^2 + 2.337 \times 10^{-8} T + 3.445 \times 10^{-7} \quad (8)$$

where viscosity is in [Pa.s] units, temperature in [K]. Dependence, described by Eq. (3), was derived by extrapolation based on the hydrocarbons viscosity values. Actually, due to relatively low flow rates of the precursor, the viscosity of mixture was closer to the carrier (Ar) viscosity ( $\eta_{mixture} \approx \eta_{Ar}$ ). We used weighted viscosity in computation according relationship

$$\eta_{mixture} = \frac{1}{p_{total}} \sum_s \eta_s p_s \quad (9)$$

with index (s=Ar, EGDA, TBPO and TBPO radicals). Density of mixture is given by

$$\rho_{mixture} = \sum_s n_s m_s \quad (10)$$

Precursors transport through reactor was computed assuming convection and diffusion mechanisms. Diffusion coefficients for precursor molecules of the “s-kind” in argon are estimated by expression

$$D_s = \frac{1}{3\pi} \frac{\sqrt{8kT/\pi m_s}}{\sqrt{2n_s D_s^2 + n_{Ar} D_{Ar-s}^2} \sqrt{m_s/m_{Ar-s}}} \quad (11)$$

where  $m_{Ar-s} = m_{Ar} m_s / (m_{Ar} + m_s)$  and index “s” has previous meaning.

### Boundaries

Sources of EGDA and TBPO were set within boundary conditions as a constant concentration at the inlet boundaries. As we mentioned above, this work relates to significantly simplified chemistry, though model is pre-formulated to distinguish between various internal surfaces and their physical properties. Sticking coefficients of all species were set to value  $10^{-6}$  on internal surfaces excluding the surface of NiCr and wafer surface. To mimic the TBPO decomposition on hot surface the sticking coefficient was set to unity at surface of the heated NiCr elements. On the other hand, the radicals were considered they do not stick to NiCr (sticking coefficient is zero).

Monomer sticking coefficient was estimated from deposition rate shown in Fig. 3-a. Starting from preset value  $10^{-6}$  we iterate simulations of the EGDA-TBPO system at given conditions to achieve experimental value of the deposition rate  $\sim 0.74$  nm/s. In this manner we determined an empirical sticking coefficient of the molecule EGDA in a form

$$\zeta_{EGDA} \approx 0.023 + 0.00137/T \quad (12)$$

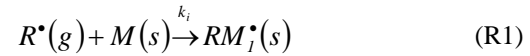
or in more convenient form

$$\zeta_{EGDA} \approx 0.023 \exp(0.5945/T) \quad (13)$$

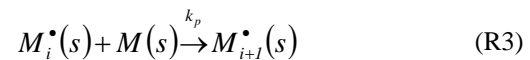
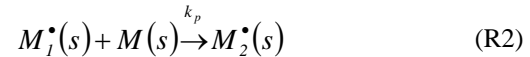
In related work<sup>20</sup> the sticking coefficient under similar conditions but different monomer was used - poly(cyclohexylmethacrylate), pCHMA – was estimated from the coverage of the microtrenches in the range from 0.011 to 0.05. Our result falls into the middle of this interval. From relation (13) we determined also the effective activation energy of “a polymerization”, which was about 4.94 J/mol for iCVD mode.

### Surface Chemistry

Geometry (size of the filament area) will have effect on production of the radicals. Volume recombination of the radicals is set to be negligible. Understanding and correct description of the surface reactions is crucial in polymerized film growth. Boundary conditions are considering surface model that assumes various fractional coverage by “growing / passivating” surface sites. Firstly, creating surface sites occurs by adsorption at surface. We are assuming *non-dissociated physical adsorption* in all cases both for initiator and monomer. Reduced set of surface chemistry is represented by following reactions: The initiation of monomer by TBPO radicals is described by reaction



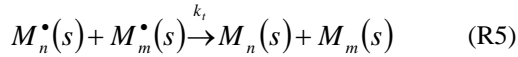
Then film growth continues through a multi-step propagation chain



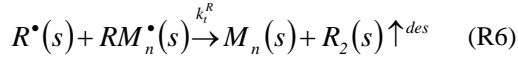
And, finally, film growth termination is completed by several reactions, for example, in association mode



the quenching mode

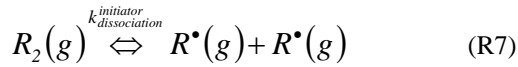


and the radical recombination mode

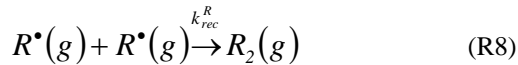


In other words, the polymer film is gradually growing from produced surface sites by sequence initiation  $\rightarrow$  propagation  $\rightarrow$  termination (IPT sequence).

In gaseous phase we included decomposition of the initiator into two radicals (though, under given conditions and involved chemistry they are less significant).



Using the experimental results,<sup>9</sup> an activation energy for TBPO decomposition was set to 163 kJ/mol. The reverse reaction is a recombination of two radicals



We formulated system of equations that described the fractional coverage of the surface sites. Attempt to solve such system analytically failed due to non-linear members and giving non-physical solutions. Much significant reduction of the surface model, eliminating intentionally surface reactions that are due to Langmuir-Hinshelwood mechanism (these create non-linearity), keeping only Eley-Rideal mechanism we were able to obtain the analytical solution and incorporate it into boundary conditions. The second approach – to set required surface reactions into FEI model to solve case numerically – is part of further development in this topic. Though, our concern is that problem with cyclic variable may occur. Another concern is that in either approaches, analytical or numerical, our limiting factor was the absence of a knowledge of the appropriate rate constants and sticking probabilities, and this in part will have to be gained by experimentation.

#### 4. Results and Discussion

As we mentioned in an introduction section, this study is part of the larger developmental work and currently is going through the earlier phases – main goal of which was to develop a suitable computational model for FACVD/Icvd

processes capable to describe and obtain with reasonable accuracy all or at-least some of the most critical and relevant phenomena occurring in the reaction chamber. In this section we will expose only some aspects of this study. The baseline type of study is documented on the next several pictures.

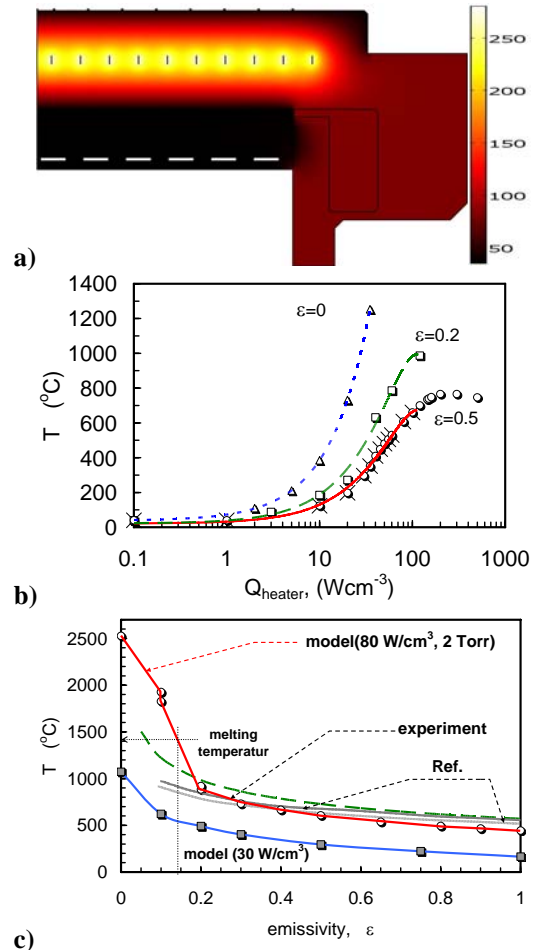


**Figure 8.** Results of the heat transfer model simulation: (a) Temperature distribution inside reactor with well illustrated hot zone. Surface plot scale is in °C.; (b) Ribbon temperature vs. heating power considering various emissivity of NiCr surface; (c) Comparison of the modeled ribbon temperature vs. emissivity to measurement in reactor and to the published experimental data.<sup>18</sup>

Typical thermal distribution in reactor is shown in Fig. 8-a. Involving radiation heat transport gave us opportunity to scale modeled data more realistic with experimental measurements. Radiosity from ribbons does not

have an eminent impact on the temperature distribution but calibrates temperature range more correctly. Neglecting the radiation brings ribbon temperature much higher values due to low heat loss under vacuum conditions.

Dependence of the heater temperature vs. electrical power is shown in Fig. 8-b. In dependence on the NiCr surface status (that means, the actual value of the emissivity) the prediction of the operational range for  $\sim 300$  °C process (for example, TBPO molecules decomposition in iCVD) is from 10 to 40 W/cm<sup>3</sup>. To operate in 800 – 900 °C temperature interval (cracking a monomer in FACVD) it is from 50 to 100 W/cm<sup>3</sup>. Exercising the thermal model assist us in calibration with experimental data.

The emissivity value is critical. It can vary over the heater lifetime time due to a degradation of the surface properties. Examination of thermal performance vs. NiCr emissivity (Fig 8-c) showed agreement with experimental data and qualitative superposition with observation done by other investigators.<sup>18</sup> In interval  $\epsilon > 0.2$ , the modeled curve (80 W/cm<sup>3</sup>, red) overlays both experimental data<sup>21</sup> (green curve) and published data (gray curves). Below  $\epsilon < 0.2$ , model shows increased temperature, due to elimination of the radiation losses.

Simulated temperature is exceeding even melting point for NiCr, which is absolutely correct, since we did not assume melting effect in model. However, this has practical implication, it indicates the condition when NiCr heater could fail in real reactor. That means low-emissivity NiCr surface (typically, when it is oxidized) could generate failure of heater.

Surface plot series in Fig. 9 show concentration distribution of the EGDA monomer precursor (Fig. 9-a), initiator TBPO (Fig. 9-b) and initiator radicals (Fig. 9-c). These plots represent initial simulations. We speculated that structured appearance of the concentrations plots for heavy molecules like EGDA and TBPO was due to several reasons. One could indicate that heavy molecules are dragged by convection flow, and not spreading instantly by diffusion transport, which from the plots seems to be very low.

Another cause could be, that our approach in the estimate of a diffusivity is underestimating the real diffusion coefficient. As we found out later during a development process, the diffusion

coefficients were actually underestimated. We estimated  $D_s$  based on mean-free-path kinetic derivation, which may not be the most accurate way to proceed. Nevertheless, the qualitative aspects are reflecting process correctly.

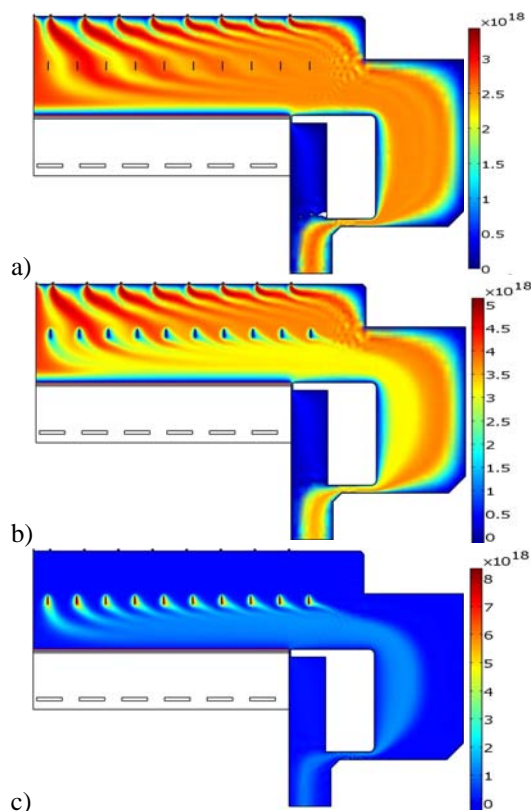


**Figure 9.** Concentration plots inside reactor in the case: (a) precursor (EGDA); (b) initiator TBPO (parental molecules), and produced radicals of TBPO within hot zone and their transport towards the wafer surface. Total pressure was 2 Torr. Colored surface plot scales are in [m<sup>-3</sup>] units.

For example, qualitatively anticipated result follows from Fig. 9-b and Fig. 9-c. The concentration of the TBPO is depleted in location of the heater assembly, close to the ribbon surface. This is due to the increased losses in this zone and decomposition of the TBPO into radicals. Consequently, the radicals TBPO are originating on the ribbon surface (see, Fig. 9-c).

The surface plots post processed from the most recent simulation are given in Fig. 10, where EGDA, TBPO and its radicals are plotted at the identical conditions as simulation brought

in Fig. 9. Diffusivity of the components is much higher providing uniform distribution of the molecules above the substrate (see image on deposited film at the 300 mm wafer in bottom/right corner).

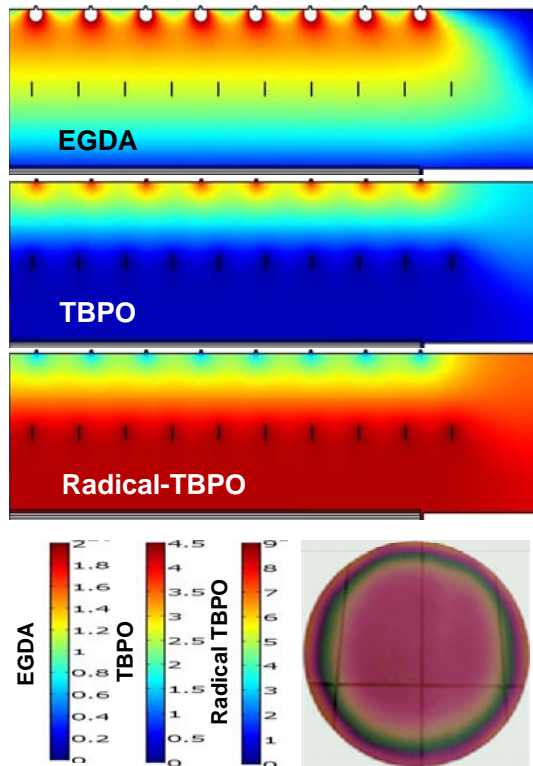


**Figure 10.** Simulation plots of the concentration of EGDA, TBPO and TBPO at 2 Torr iCVD conditions. Plot scales are in  $[10^{18} \text{ m}^{-3}]$  units. BOTTOM/RIGHT: optical image of the film as deposited onto 300 mm wafer.

In Fig. 11 several quantities are shown to illustrate iCVD process in given geometry. Surface height plot (above the background geometry plane) belongs to the EGDA concentration, which is the highest at the inlets into the reactor and dropping towards the pump outlet. Color of the surface illustrates the temperature of mixture – brighter color corresponds to the hot zone in the reactor. Streamlines orientation shows EGDA transport from the inlets towards the wafer, they are only moderately affected by the carrier gas flow. Streamlines color reflects the EGDA flux intensity – which is uniform above the wafer. Streamlines height above the background plane illustrates the TBPO radicals concentration,

which is minimal at the inlets, local peaks shows it is produced at the heating elements and it is reaching uniform distribution above the wafer surface.

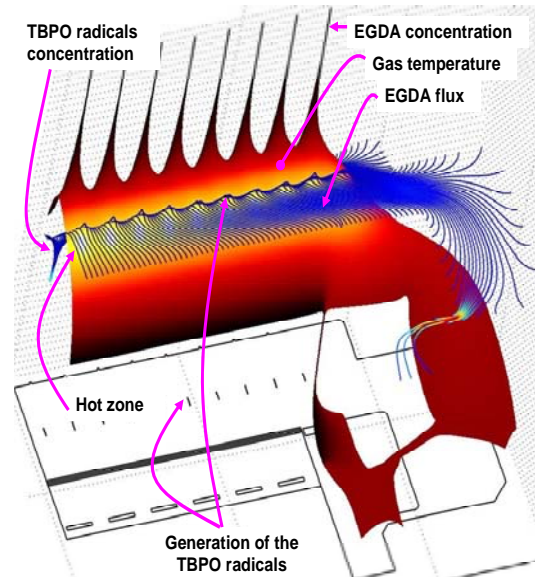


**Figure 11.** Composed plots in 3D view of the EGDA concentration (surface height plot) and its flux (streamlines color and orientation), the gas temperature (surface color plot), the TBPO-radicals (streamlines height plot). Total pressure was 2 Torr. Plots dimensions are scaled into image size. In background the corresponding geometry is depicted.

#### 4. Conclusions

FACVD is a plasma-free vacuum technology capable of producing films suitable for advanced interconnects. The flexibility of this technology allows the plasma-free deposition of polymers and dielectrics at low temperatures. In this work we developed a pivotal model for FACVD/iCVD reactor under Multiphysics Comsol sw environment. Described model can provide predictive results on FACVD (or iCVD) reactor and process performance. We used experimental results to estimate unknown parameters in the model. The effective activation energy of the “polymerization” was estimated about 4.94 J/mol for EGDA iCVD mode, and sticking coefficient of EGDA monomers about 0.023. There are still more unknown parameters, model is not perfect, and it is using several adjusted constants. We believe, this will be resolved in time, when more experimental data will be obtained from the

iCVD experiments. In virtual reactor, the film properties and process may be adjusted by simple changes to FACVD process parameters. On engineering side, the predicted thermal performance is in good agreement with experiments. Significant more development has to be done in respect to surface chemistry description and it is getting addressed in current work with more attention. Also experimental results are gradually collected to accomplish thorough full validation of the FACVD model. Thus, future systematic investigations will be focused on surface model development to assist

the optimization of DP and OSG cap layer films for Cu/low-k air gap integration and exploration of FACVD for other applications.

### Acknowledgements

The author would like to thank to his colleagues Jacques Faguet, Eric Lee, Dorel Toma and Akiyama Osayuki for fruitful discussions about FACVD processes, technological and application insights, access to the experimental data and overall opportunity to contribute to this challenging project.

### 8. References

1. J. Faguet, E. Lee, J. Liu, J. Brcka and O. Akiyama, Novel Dielectric Deposition Technology for Advanced Interconnect with Air Gap, *Proc. IEEE Int. Interconnect Technology Conference*, 35-37, (2009).
2. J.R. Hollahan and R.S. Rosler, *Ch. IV-1 in Thin Film Processes*, J.L. Vossen and W. Kern, Eds. New York, Academic Press (1978).
3. T. Sugano, Applications of Plasma Processes to VLSI Technology, John Wiley & Sons New York, 185-203 (1985).
4. H. Yasuda and T. Hsu, Some aspects of plasma polymerization investigated by pulsed R.F. discharge, *J. Polymer Sci.: Polymer Chem. Ed.* **15**, 81-97 (1977).
5. L.G. Gosset, et al., General review of issues and perspectives for advanced copper interconnections using air gap as ultralow-materials, *Proc. IEEE Int. Interconnect Technology Conference*, 65-66 (2003).
6. R. Daamen, et al., Air gap integration for the 45 nm node and beyond, *Proc. IEEE Int. Interconnect Technology Conference*, 240-242 (2005).
7. K.K.S. Lau, K.K. Gleason, Initiated Chemical Vapor Deposition (iCVD) of Poly(alkyl acrylates): An experimental Study, *Macromolecules* **39**, 3688-3694 (2006).
8. K.K.S. Lau, K.K. Gleason, Initiated Chemical Vapor Deposition (iCVD) of Poly(alkyl acrylates): A Kinetic Model, *Macromolecules* **39**, 3695-3703 (2006).
9. G. Ozaydin-Ince, K.K. Gleason, Kinetic Studies of Initiated Chemical Vapor Deposition of Polymer Nanocoatings, *MRS Proc.* (2008).
10. G. Ozaydin-Ince, K.K. Gleason, Transition between kinetic and mass transfer regimes in the initiated CVD from ethylene glycol diacrylate, *J. Vac. Sci. Technol.* **A27**(5), 1135-1143 (2009).
11. M.Olivas-Martinez, M.Perez-Tello, R. Cabanillas-Lopez, O. Contreras-Lopez, G. Soto-Herrera and F. Castillon-Barraza, A computational model for the hot filament CVD process to produce diamond films, *Modelling and Simulation in Materials Science and Engineering* **15**, 237-2261 (2007).
12. R. Bakker, V. Verlaan, A.D. Verkerk, C.H.M. van der Werf, L.van Dijk, H. Rudolph, J.K. Rath and R.E.I. Schropp, Heat transfer model of an iCVD reactor, *Thin Solid Films*, (2009), doi:10.1016/j.tsf.2009.01.030
13. <http://sigmaaldrich.com/catalog/> (2009).
14. Knovel Critical Tables, 2<sup>nd</sup> Edition (2008).
15. [www.chemexper.com/chemicals/supplier/](http://www.chemexper.com/chemicals/supplier/) (2009).
16. J. Brcka and J. Faguet, Analysis of the thermal and gas flow performance of the multi-linear planar heater for 300 mm wafer FACVD technology, *TEL Technology Symposium*, Nirasaki-Yamanashi, Japan (2008).
17. Y.S. Touloukian and D.P. DeWitt, Thermal Radiative Properties - Metallic Elements and Alloys, *Thermophysical Properties of Matter*, IFI/Plenum, New York (1970).
18. J. Zhou, T.R. Ohno, and C.A. Wolden, The high temperature stability of nichrome in reactive environments, *J. Vac. Sci. Technol.* **A21**(3), 756-761 (2003).
19. TBPO – obtained from Knovel database
20. S.H. Baxamusa, K.K. Gleason, Initiated Chemical Vapor Deposition of Polymer Films on Nonplanar Substrates, *Proc. 5<sup>th</sup> Int. Conf. on HWCVD*, MIT, Cambridge (2008).
21. TEL internal results, J. F<sup>1</sup>aguet (2009).